

# Multi-fidelity Fluid-Structure Interaction Analysis of a Membrane Wing

M. Saeedi, R. Wüchner, K.-U. Bletzinger

**Abstract**—In order to study the aerodynamic performance of a semi-flexible membrane wing, Fluid-Structure Interaction simulations have been performed. The fluid problem has been modeled using two different approaches which are the vortex panel method and the numerical solution of the Navier-Stokes equations. Nonlinear analysis of the structural problem is performed using the Finite Element Method. Comparison between the two fluid solvers has been made. Aerodynamic performance of the wing is discussed regarding its lift and drag coefficients and they are compared with those of the equivalent rigid wing.

**Keywords**—CFD, FSI, Membrane wing, Vortex panel method.

## I. INTRODUCTION

**F**LEXIBLE wings have been the topic of many research programs. Different techniques have been used in order to bring flexibility to conventional wing configurations. They range from using new structural concepts for wing frame like telescopic spars [1] or morphing wing [2] to using smart materials in manufacturing of the wing [3]. In active control concepts like morphing wing, deformability is brought to the wing by the use of actuators, in passive control on the other hand the wing is to some extent flexible and is deformed solely as a consequence of applied aerodynamic loads. In the case of passive control the final form of the wing is a result of the equilibrium between aerodynamic forces and internal structural forces and therefore it is not trivial to reach the desired final form. Membrane wings are also a good alternative to rigid wing constructions for Micro Air Vehicles (maximum dimension of 15cm by definition) [4], [5]. The flexibility of a membrane wing enables it to adapt itself to the flow field to a certain extent. The advantages of this passive adaption to the surrounding flow are from aerodynamics point of view a higher lift slope, higher maximum lift coefficient and postponed stall to higher angles of attack compared to rigid wings [6] and from the structural perspective load reduction in unsteady flow cases [7]. One drawback of flexible wings could be that because of their flexibility and due to self excited vibrations they could show unsteady response even to steady flow conditions [8].

A membrane wing concept is studied in the current work. Membrane structures are able to efficiently carry external loads over large spans via internal in-plane stresses. The response of such a wing to aerodynamic loads depends on the membrane's stresses, so two-way coupled fluid-structure

interaction simulations (FSI) are necessary to analyze its performance. Numerous simulations might be needed to find the best set of prestresses to ensure a better aerodynamic performance. It highlights the need for less complex fluid models for FSI simulations during early design stages. An alternative to the numerical simulation of the flow field using Navier-Stokes equations (NSE) is the vortex panel method. The panel method is computationally less demanding and enables faster exploration of the design space. However, in general, it neglects viscous effects and therefore its range of applicability should be evaluated. In the current paper FSI simulations for the membrane wing concept have been performed using the two approaches for the fluid side and the results are compared. Aerodynamic performance of the membrane wing is compared with its equivalent rigid wing as well.

## II. MEMBRANE WING CONCEPT AND FSI SIMULATION STRATEGY

Fig. 1 shows the membrane wing concept studied in the current work. The sailwing concept was proposed by Ormiston during the 80s [9]. A rigid mast forms the leading edge section of the wing. To support the upper and lower membranes, spars are mounted along the span of the wing and their number depends on the span length of the wing. Upper and lower membranes are joined together at the trailing edge via a pretensioned edge cable.

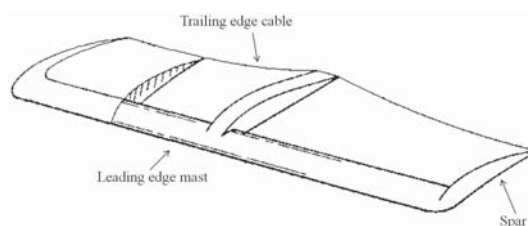


Fig. 1 Sailwing construction concept, from [9]

In case of a flexible membrane wing, the shape of the wing surface depends on the one hand on the working conditions in terms of wind speed, angle of attack, etc. and on the other hand on the structural properties of its supporting frame and the membranes which form the wing surface. Pressure distribution on the surface of the wing depends on the form and the above mentioned working condition. Structural properties of the wing govern its deformation under such a loading. The final form of the wing results from this interaction between loading and displacement. This emphasizes the necessity of

M. Saeedi is with the Chair of Structural Analysis, Technical University of Munich, Germany (e-mail: mehran.saeedi@tum.de).

R. Wüchner is with the Chair of Structural Analysis, Technical University of Munich, Germany (e-mail: wuechner@tum.de).

K.-U. Bletzinger is the head of the Chair of Structural Analysis, Technical University of Munich, Germany (e-mail: kub@tum.de).

FSI simulations for the analysis of such a wing concept. FSI simulations are computationally complex and time-consuming. From the fluid point of view, turbulent flow should be simulated using either LES or RANS turbulence models and on the structural side nonlinear dynamic or static analysis is needed in order to correctly deal with large displacements which occur in membrane wings. The analysis starts with form finding simulation. In form finding the equilibrium state of the wing is calculated, i.e. the state where membrane and edge cable internal forces are in a balance is computed. This is typically the initial shape of the wing surface in the absence of external forces. FSI simulations are started from this initial state. In the following, fluid, structure and coupling related aspects are explained.

#### A. Fluid Model

Two different approaches are used for the modeling of fluid flow. The first one is the numerical solution of Navier-Stokes equations using the finite volume method and the second one is the vortex panel method. The advantage of the vortex panel method is that it is computationally less demanding, while its drawback is that it neglects the viscous effects. Still it is a very good alternative to Navier-Stokes during the early design stages. While a steady state FSI simulation using the first approach takes about 15 hours to converge, the same simulation takes about 20 minutes to converge to the steady-state solution using vortex panel method. Even though some details of fluid flow are neglected in vortex panel method, the fact that it is much faster than solving Navier-Stokes equations enables design space explorations at reasonable computational costs in a certain range of operating conditions

1) *Navier-Stokes Equations:* The NS equations are the general equations describing the flow of fluid substances. For flows with constant viscosity they read:

$$\nabla \cdot (\rho \mathbf{v}) = 0 \quad (1)$$

and

$$\rho \left( \frac{\partial \mathbf{v}}{\partial t} + \mathbf{v} \cdot \nabla \mathbf{v} \right) = -\nabla p + \mu \nabla^2 \mathbf{v} + \mathbf{f}. \quad (2)$$

Velocity ( $\mathbf{v}$ ) and pressure ( $p$ ) fields are coupled in these equations. SIMPLE algorithm of Patankar and Spalding [10] is used to enforce the coupling. Reynolds averaged Navier-Stokes model is used for turbulence modeling and turbulent viscosity is modeled using  $k - \omega SST$  model [11]. It is a two equation model used to calculate kinematic eddy viscosity. First the equations for turbulent kinetic energy ( $k$ ) and specific dissipation rate ( $\omega$ ) are solved. Kinematic eddy viscosity is then calculated from  $k$ ,  $\omega$  and other parameters of the model.

2) *Vortex Panel Method:* The velocity field for the case of irrotational, incompressible and inviscid flow can be represented by a velocity potential  $\Phi$ . This is the basis for vortex panel method. The flow velocity can be calculated from the potential in the following way:

$$u = -\frac{\partial \Phi}{\partial x}, \quad (3)$$

$$v = -\frac{\partial \Phi}{\partial y}, \quad (4)$$

$$w = -\frac{\partial \Phi}{\partial z}. \quad (5)$$

Inserting the above equations into continuity equation (1) results in the continuity equation in terms of the potential:

$$\nabla^2 \Phi = 0. \quad (6)$$

This equation can be solved by superposition of elementary solutions. There are two boundary conditions for solving this Laplacian equation. One is that at no-slip walls in the domain (e.g. on wing surface) the velocity component normal to the surface should vanish:

$$\nabla \Phi \cdot \mathbf{n} = 0, \quad (7)$$

where  $\mathbf{n}$  is the vector normal to the surface. The other condition is that the disturbance in the freestream flow caused by the elementary solutions should vanish as the distance,  $r$ , from the boundary surface increases:

$$\lim_{r \rightarrow \infty} \nabla \Phi = 0. \quad (8)$$

Using the Green's identity it can be shown that the potential at each point,  $P$ , inside the domain can be calculated in terms of the potential ( $\Phi$ ) and its derivative ( $\frac{\partial \Phi}{\partial \mathbf{n}}$ ) on the boundary of the domain:

$$\Phi(P) = \frac{1}{4\pi} \int_S \left( \frac{1}{r} \nabla \Phi - \Phi \nabla \frac{1}{r} \right) \cdot \mathbf{n} dS \quad (9)$$

Detailed derivation of (9) is available in [12]. The problem is now reduced to finding the values of the potential on the boundary which fulfill the continuity equation (6) and the two boundary conditions stated in (7) and (8). Laplace equation is a linear equation and if two functions fulfill the equation, their linear combination fulfills the equation as well. Hence, the solution of the continuity equation can be found as a superposition of elementary solutions like sources and doublets on the boundary of the domain. For a point source with strength of  $\sigma$  we have:

$$\Phi = -\frac{\sigma}{4\pi r} \quad (10)$$

and

$$\mathbf{v}(P) = \frac{\sigma}{4\pi} \frac{\mathbf{r}}{r^3} \quad (11)$$

where  $\mathbf{r}$  is the vector from the point source to the point  $P$  and  $r$  is its magnitude. For a point doublet with strength of  $\mu$  the potential reads:

$$\Phi = \frac{\mu}{4\pi} \mathbf{n} \cdot \nabla \left( \frac{1}{r} \right) \quad (12)$$

and the three components of the velocity at a point  $P = (x, y, z)$  due to a point doublet located at  $(x_0, y_0, z_0)$  are

$$u = -\frac{\mu}{4\pi} \frac{(y - y_0)^2 + (z - z_0)^2 - 2(x - x_0)^2}{[(x - x_0)^2 + (y - y_0)^2 + (z - z_0)^2]^{\frac{3}{2}}}, \quad (13)$$

$$v = \frac{3\mu}{4\pi} \frac{(x - x_0)(y - y_0)}{[(x - x_0)^2 + (y - y_0)^2 + (z - z_0)^2]^{\frac{3}{2}}}, \quad (14)$$

and

$$w = \frac{3\mu}{4\pi} \frac{(x - x_0)(z - z_0)}{[(x - x_0)^2 + (y - y_0)^2 + (z - z_0)^2]^{\frac{5}{2}}}. \quad (15)$$

The elementary solutions automatically satisfy the constraint that they should decay as the distance increases. Their resulting velocity vanishes as  $r$  tends to infinity. But the velocity goes to infinity as  $r$  tends to 0. That is why they are called singular solutions. In panel method the strength of these singular solutions are calculated using the boundary condition stated in (7) to enforce zero normal velocity at the surface of the boundary. The surface of the wing is discretized with a number of panels as shown in Fig. 2. Each panel on the wing surface represents a quadrilateral source and a quadrilateral doublet element. In addition to wing panels there are wake panels to represent the wake behind the wing. Wake panels consist of quadrilateral doublets.

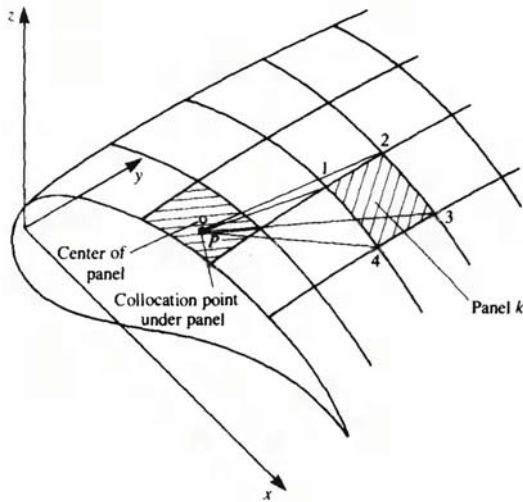


Fig. 2 Discretization of the wing surface into panels, from [12]

There are two ways to enforce the zero normal flow boundary condition. It can be enforced as a Dirichlet boundary condition by setting a constant value for the potential inside the body or as a Neumann boundary condition which deals with the derivative of the potential, i.e. the velocity. We have used the latter implementation of this boundary condition for the collocation point at each panel. The collocation point of a panel is at the center of the panel (in the case of Dirichlet boundary condition the collocation points are shifted inside the body). The velocity at collocation point  $P$  is calculated by summing up the contribution of each panel to the velocity at this point:

$$\mathbf{v}(P) = \sum_{k=1}^N \mathbf{C}_k \mu_k + \sum_{l=1}^{N_w} \mathbf{C}_l \mu_l + \sum_{k=1}^N \mathbf{B}_k \sigma_k, \quad (16)$$

where  $N$  is the number of panels on wing's surface and  $N_w$  is the number of wake panels. The first term in (16) is for the contribution of doublet elements on the wing panel, the second represents the contribution of doublet element at the wake and finally the last one is for source terms on the wing.

$\mathbf{C}_k$  can be interpreted as the velocity caused by the  $k^{th}$  panel at point  $P$ , it is calculated for a panel of unit strength. The same interpretation holds for  $\mathbf{B}_k$  regarding the source terms. For more details on the calculation of the influence coefficients  $\mathbf{C}_k$  and  $\mathbf{B}_k$  we refer the reader to [12]. The total velocity at the point  $P$  is the velocity caused by the panels plus the free stream velocity. To set the total velocity in the normal direction to the panel to zero, the contribution of panels should cancel out that of the free stream velocity:

$$\left( \sum_{k=1}^N \mathbf{C}_k \mu_k + \sum_{l=1}^{N_w} \mathbf{C}_l \mu_l + \sum_{k=1}^N \mathbf{B}_k \sigma_k \right) \cdot \mathbf{n} = -\mathbf{v}_\infty \cdot \mathbf{n}. \quad (17)$$

Equation (17) should hold at every collocation point. Applying this equation to each collocation point we end up with a system of  $N$  equations with  $N$  unknowns. This system of linear equations is then solved for the unknowns which are the strengths of the doublet panels. It should be mentioned that the strength of the  $k^{th}$  source panels is already set to

$$\sigma(k) = \mathbf{v}_\infty \cdot \mathbf{n}(k) \quad (18)$$

and is moved to the right hand side before solving the system of linear equations.  $\mathbf{v}_\infty$  is the free stream velocity vector. The strength of wake panels is also calculated in terms of doublet strength at the upper and lower neighboring panels of the trailing edge (Fig. 3) using the Kutta condition.

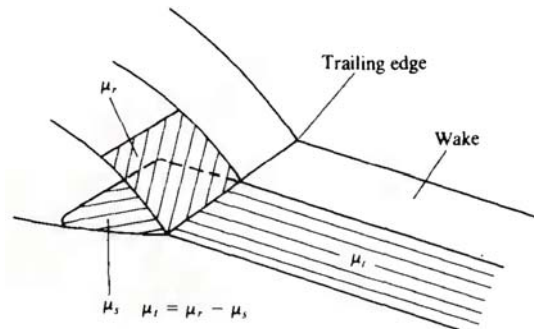


Fig. 3 Wake panels used to apply the Kutta condition, from [12]

The Kutta condition implies that the circulation at the trailing edge should be zero. Three panels intersect at the trailing edge. These are the wake panel and the two wing panels on the upper and lower surface of the wing. The Kutta condition is satisfied by setting the difference in the strength of upper and lower panel to wake strength:

$$\mu_w = \mu_{upper} - \mu_{lower}. \quad (19)$$

Strength of the doublet panels are calculated by solving the resulting system of linear equations. In the post-processing step the velocity at the points of interest, which are the collocation points in particular, is calculated. The pressure is then calculated from the steady state Bernoulli equation. Using the Bernoulli equation, the pressure coefficient reads:

$$c_p = \frac{p - p_\infty}{\frac{1}{2} \rho V_\infty^2} = 1 - \left( \frac{\|\mathbf{v}\|}{\|\mathbf{v}_\infty\|} \right)^2. \quad (20)$$

Fig. 4 shows the calculated pressure distribution at the middle section of a NACA0012 wing for an angle of attack of 6 degrees. The results are compared with the ones from XFLR5 [13].

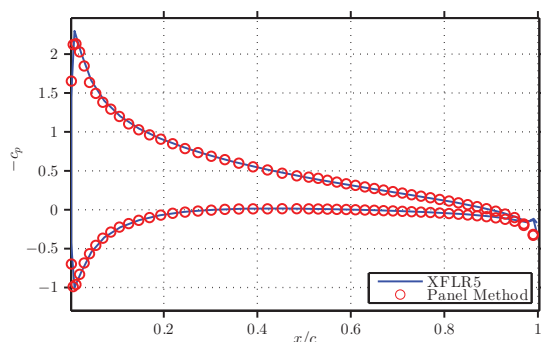


Fig. 4 Pressure distribution over a NACA0012 wing section,  $\alpha = 6^\circ$

### B. Structural Model

Structural analysis of the membrane wing consists of two steps: Form Finding and Nonlinear Static analysis.

In structural analysis the finite element method is used and displacements are calculated for a specific structure under applied load. Form Finding of membrane structures can be seen as the inverse problem of structural analysis. Prestressed membrane structures are usually supported at the edges by pretensioned edge cables. In the inverse problem of form finding the stresses in membrane and edge cables are given and support conditions (fixed boundaries) are defined. The goal of the form finding analysis is to find the shape at which an equilibrium between structural forces exists. In other words, form finding analysis calculates the equilibrium shape of the membrane enclosed by a given boundary and with predefined stress distributions. It has been inspired by the works of the German architect, Frei Otto [14], and was originally developed for form finding of cable structures. Form finding could be done using different approaches like Force Density Method [15], Dynamic Relaxation [16] or Updated Reference Strategy (URS) [17], [18]. We have used the URS based method available in the in-house structural solver CARAT++. As a classical form finding example, the 4 point tent is presented in Fig. 5.

CARAT++ has also been used for performing static nonlinear analysis using the load-control method.

### C. FSI Simulation Strategy

In order to link the fluid solver (OpenFOAM) to the structural solver (CARAT++) for the partitioned analysis of the FSI problem [19] a coupling tool is needed. The coupling is done using an in-house coupling tool called EMPIRE.

The coupling tool takes care of the communication between the two solvers. At each iteration it first receives the discretized pressure field from the fluid solver. The structural solver needs nodal forces to calculate displacements. The

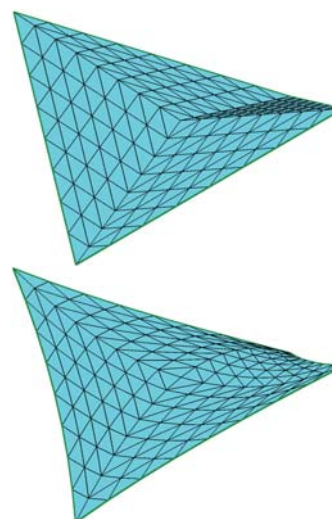


Fig. 5 Form finding analysis of a 4 point tent. Top: initial state. Bottom: equilibrium state

coupling tool maps the pressure from fluid mesh to structure mesh, calculates the equivalent nodal force and sends it to the structural solver. The structural solver then calculates displacement field, the coupling tool receives the calculated displacement and sends it to corresponding nodes of the fluid mesh. The fluid solver applies the received displacement to its mesh and proceeds to the next iteration. For a steady state problem this iterative procedure is repeated until it is converged to the steady state solution.

## III. RESULTS

The studied wing with S809 airfoil profile can be seen in Fig. 6. It has a span of 4.5m and a uniform chord length of 1m along the span. Dihedral and sweep angles are both zero. Upper and lower membranes are wrapped around the rigid leading edge which extends up to 10% of the chord. The membranes are supported by 4 spars and by an edge cable at the trailing edge. The 4 spars divide the wing into 3 uniform segments. Structural properties of the membranes, spars (which are modeled as beams) and edge cable are summarized in Tables I to III.

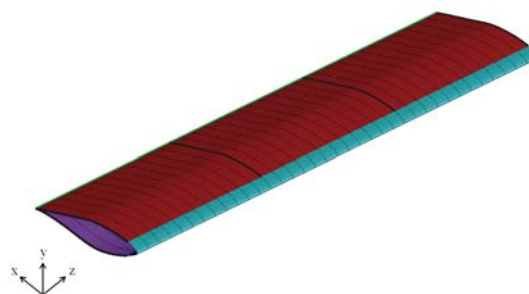


Fig. 6 Wing planform

TABLE I: MEMBRANE PROPERTIES, (U: UPPER, L: LOWER )

$E$	84MPa
$\rho$	1400kg/m <sup>3</sup>
$t$	0.48mm
$\sigma_{chordwise}^u$	300kPa
$\sigma_{spanwise}^u$	1600kPa
$\sigma_{chordwise}^l$	300kPa
$\sigma_{spanwise}^l$	1600kPa

TABLE II: TRAILING EDGE CABLE PROPERTIES

$E$	125GPa
$\rho$	7800kg/m <sup>3</sup>
radius	4mm
$\sigma$	50MPa

TABLE III: BEAM PROPERTIES

$E$	190GPa
$\rho$	7800kg/m <sup>3</sup>
$A$	2cm × 12cm

9 shows the discretized computational domain used for CFD simulations. It consists of 2.9 million hexahedral cells, which results in a  $y^+$  value of about 70. To check if the mesh is fine enough, the results of the Reynolds number of  $Re = 10^6$  are compared with the experimental and numerical results reported in [20]. The comparison has been made only up to an angle of attack of  $9^\circ$ , for higher angles of attack a finer mesh could be needed to properly capture stall effects.

### A. Form Finding

The equilibrium state of the wing with structural parameters presented in the Tables I to III is calculated in a form finding analysis. The deformed state is compared with the reference state in Fig. 7. Membranes and the edge cable pull against each other and as a result, the edge cables are moved toward the leading edge with maximum displacement at the middle of each wing segment. The prestresses in the membranes form double-curved surfaces, where the upper membranes are moved downwards and lower membranes are moved upwards. While the cross section remains unchanged at the 4 spars, due to the deformation of the two membranes, the cross section of the wing changes continuously on other sections along the span. Fig. 8 also shows how the cross section at the middle of the wing deviates from the initial S809 profile.

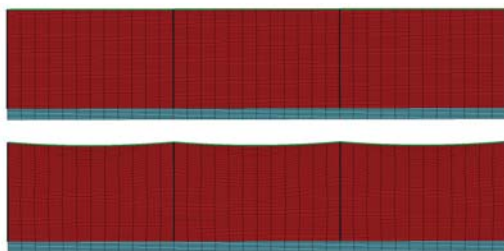


Fig. 7 Form finding of the membrane wing. Top: initial state. Bottom: equilibrium state

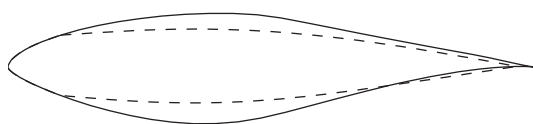


Fig. 8 Form finding of the membrane wing (mid-span section). Solid line: initial state. Dashed line: equilibrium state

### B. Fluid Setup

For the fluid side, SimpleFoam solver from OpenFOAM has been used for performing steady state CFD simulations. Fig.

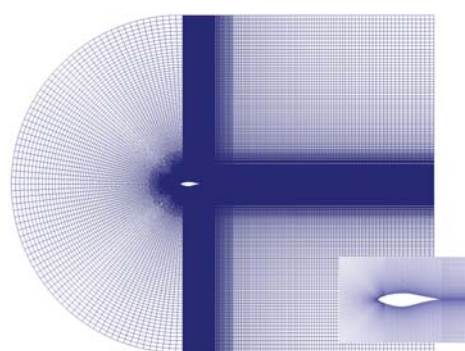


Fig. 9 Computational domain

The  $k - \omega SST$  model has been used. OpenFOAM wall functions are used at wing surface,  $kqWallFunction$  for  $k$  and  $\omega wallFunction$  for  $\omega$ . The velocity at the inlet is  $30m/s$  which corresponds to a Reynolds number of  $2 \times 10^6$

### C. FSI Simulations

FSI simulations have been done for 7 different angles of attack from  $0^\circ$  to  $9^\circ$  with an increment of  $1.5^\circ$ . Convergence to steady state solution for the case of using panel method solver is about 25 times faster than simpleFoam solver. For both cases a relaxation factor of 0.15 has been used for the displacement field. First, we compare the convergence behavior of the displacements for each approach to the steady state solution (Fig. 10). Displacement in  $y$  direction for the point at the mid-span section of the wing with  $x/c = 0.5$  is compared ( $c$  is the chord length). While with the panel method convergence is reached within 20 iterations, FSI simulation using SimpleFoam takes 450 iterations to converge. The time each iteration takes is also different in the two approaches. Overall, in case of the panel method convergence is reached approximately 25 times faster. For this particular case FSI\_CFD simulation has taken about 7.5 hours to converge using 4 processors, but FSI\_panel has converged within about 20 minutes on a single processor of the same machine. For  $\alpha = 3^\circ$  the converged displacement is  $0.033m$  from FSI\_panel and  $0.035m$  from FSI\_CFD.

The comparison of the two approaches for the selected point is summarized in Table IV. For  $\alpha = 0^\circ$  both approaches result the same displacement. It is not the case for higher angles of attack as the panel solver tends to underpredict the overall

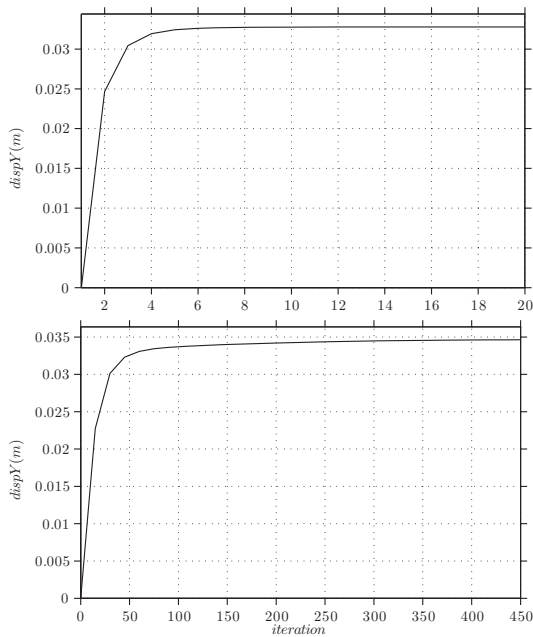


Fig. 10 Convergence of the displacement for a selected point. Top: FSI\_Panel. Bottom: FSI\_CFD

TABLE IV: COMPARISON OF DISPLACEMENT (m) IN  $y$  DIRECTION FOR DIFFERENT ANGLES OF ATTACK

$\alpha$ (deg)	FSI_Panel	FSI_CFD	%diff
0	0.028	0.028	0
1.5	0.030	0.031	3.22
3	0.033	0.035	5.71
4.5	0.035	0.038	7.89
6	0.038	0.040	5.00
7.5	0.04	0.041	2.44
9	0.042	0.039	7.69

pressure distribution and as a consequence, it results in smaller displacements. It is not the case for  $\alpha = 9^\circ$ . For this angle of attack the panel solver overpredicts the pressure and results in a larger displacement. It should be a result of neglecting the viscous effects, which play an important role as the flow gets closer to the stall region at  $\alpha = 9^\circ$ .

A better comparison can be made by comparing the displacement along the whole span and not only at one certain point. This has been done for the section at the mid-span of the wing (Fig. 11). For the first 4 angles of attack (up to  $4.5^\circ$ ) and especially for the upper surface of the wing there is a very good agreement between the resulting displacement from the two approaches. But from the angle of attack of  $6^\circ$ , they start to deviate from each other.

As the angle of attack increases we get closer to the stall point and viscous effects become more and more important. These effects are neglected in the panel method which causes its accuracy to decrease as the angle of attack is increased. Moreover, as the angle of attack increases, the pressure peak on the membrane part of the lower surface of the wing increases as well. The fluid pushes the membrane upward, while the leading edge part of the wing is rigid. This results in a discontinuity in the slope of wing surface, as shown

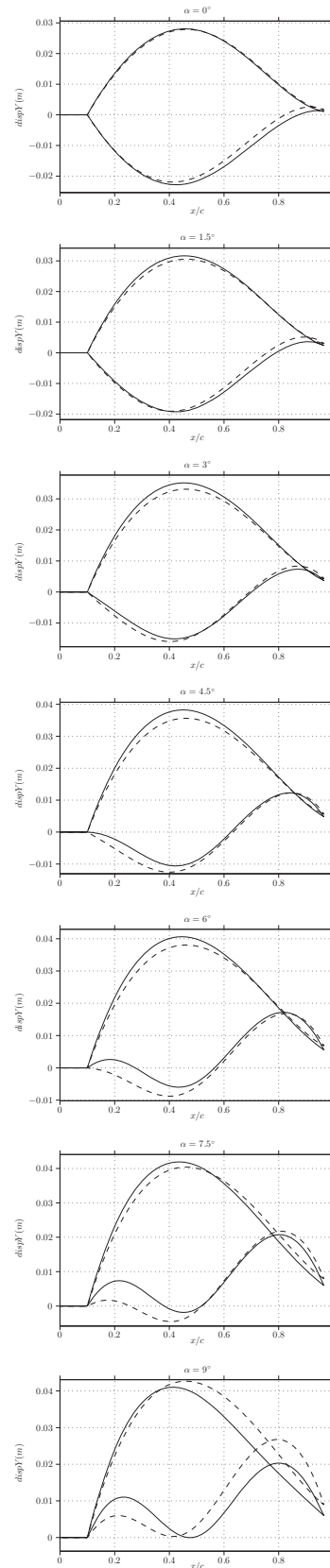


Fig. 11 Displacement in  $y$  direction along the mid-span section. FSI\_CFD: solid line. FSI\_Panel: dashed line

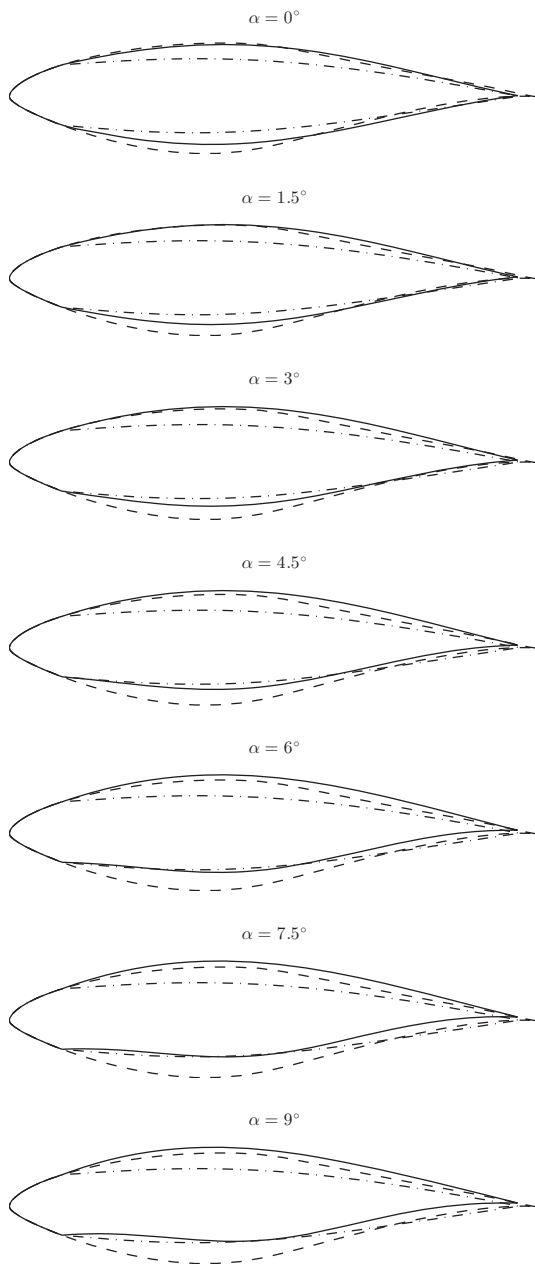


Fig. 12 Airfoil shape at the mid-span section. S809 airfoil: dashed line. Undeformed section: dot-dashed line. Deformed section: solid line

in Fig. 12, and the panel solver does not seem to be able to capture the flow physics at the kink: it overpredicts the pressure in the vicinity of the kink and consequently the resulting displacement from the two solvers deviate from each other.

Membrane wings enable a lighter wing construction and their flexibility is an advantage in terms of dynamic loading applied to the wing. It should also have an improved performance compared to rigid wing configurations in stall region because of the so called soft-stall characteristics of the membrane wing. In order to assess the aerodynamic

performance of the studied wing section, lift coefficient, drag coefficient and lift to drag ratio of the membrane wing are compared with the initial rigid wing configuration (the one before form finding). As it can be seen in Fig. 13, the drag coefficient is smaller for the whole range of studied angles of attack. At smaller angles of attack, the rigid wing has better lift characteristics than the membrane wing, but from  $\alpha \approx 2.5^\circ$  it is the membrane wing which shows a higher lift coefficient. The reason for that is mainly the flexibility of the upper surface. The upper membrane is pulled upward which increases the thickness of the wing section and causes greater lift compared with the rigid case.

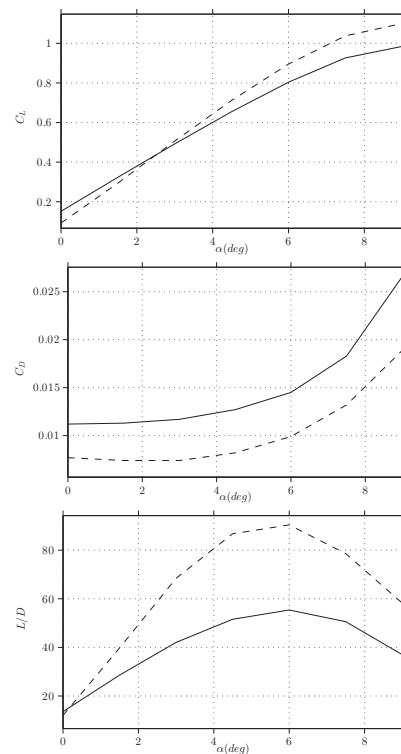


Fig. 13 Comparison of the membrane wing with the equivalent rigid wing configuration for varying angle of attack. Rigid wing: solid line. Membrane wing: dashed line

#### IV. CONCLUSION

Fluid-structure interaction simulation of a semi-flexible wing configuration has been done over a range of angles of attack. Two different fluid models have been used: CFD simulation based on RANS equations and vortex panel method. The panel method saves computation time while providing a good accuracy up to an angle of attack of  $6^\circ$ . This makes the panel method an appropriate tool for early design stages where an extensive parameter study needs to be done. Its accuracy could be improved by coupling boundary layer models to it. The studied membrane wing concept shows a higher slope of lift curve as function of angle of attack and has a better lift to drag ratio compared to the equivalent rigid wing.

## REFERENCES

- [1] Blondeau, J., Richeson, J., and Pines, J.D.: Desing, development and testing of a morphing aspect ratio wing using an inflatable telescopic spar. AIAA Paper 2003-1718, April 2003.
- [2] Bowmann, J., Sanders, B., Cannon, B., Kudva, J, Joshi, S., Weisshaar, T.: Development of Next Generation Morphing Aircraft Structures. AIAA 2007-1730, April 2007.
- [3] Barbarino, S., Dettmer W., Friswell M.: Morphing Trailing Edges with Shape Memory Alloy Rods, ICAST 2010
- [4] Lian Y., Shyy W., Numerical Simulation of Membrane Wing Aerodynamics for Micro Air Vehicle Applications, AIAA J. of Aircraft, Vol. 42, No. 4, July.-Aug 2005
- [5] Abdulrahim, M., Garcia, H., and Lind, R.: Flight Characteristics of Shaping the Membrane Wing of a Micro Air Vehicle, AIAA J. of Aircraft, Vol. 42, No. 1, Jan.-Febr. 2005
- [6] Valasek, J.: Morphing Aerospace Vehicles and Structures. John Wiley, 2.
- [7] Levin, O., Shyy, W.: Optimization of a flexible low Reynolds number airfoil. AIAA Paper 2001-16055, Jan. 2001.
- [8] Waszak, R.M., Jenkins, N.L., Ifju P., Stability and Control Properties of an Aeroelastic Fixed Wing Micro Aerial Vehicle, AIAA Paper 2001-4005, 2001.
- [9] R. Ormiston. Theoretical and Experimental Aerodynamics of the Sailwing, J. Aircraft, 1971
- [10] Patankar S.V., Spalding D.B. A calculation procedure for heat, mass and momentum transfer in three-dimensional parabolic flows. International Journal of Heat and Mass Transfer 1972,15: 1787-1806
- [11] Menter F.R. , Two-Equation Eddy-Viscosity Turbulence Models for Engineering Applications, 1994, AIAA Journal, vol. 32, no 8. pp. 1598-1605.
- [12] Katz J, Plotkin A. Low Speed Aerodynamics , Cambridge, Cambridge Univ. Press, 2008
- [13] XFLR5, <http://www.xflr5.com/xflr5.htm>, Sep. 2014
- [14] Otto F., Rasch B. Finding Form, Deutscher Werkbund Bayern, Edition A, Menges, 1995.
- [15] Schek H-J, The force density method for form finding and computations of general networks, Computer Methods in Applied Mechanics and Engineering, 1974, 3:115-134
- [16] Wakefield DS, Engineering analysis of tension structures: theory and practice, Engineering Structures, 1999, 21(8): 680-690
- [17] Bletzinger K-U., Form finding of tensile structures by the updated reference strategy, In proceedings of the IASS International Colloquium Structural Morphology-Towards the New Millennium, Chilton JW et al. (eds), University of Nottingham, U.K., 1997.
- [18] Wüchner, R. and Bletzinger, K.-U. (2005), Stress-adapted numerical form finding of pre-stressed surfaces by the updated reference strategy. Int. J. Numer. Meth. Engng., 64: 143166
- [19] Wüchner, R., Kupzok, A. and Bletzinger, K.-U. (2007), A framework for stabilized partitioned analysis of thin membranewind interaction. Int. J. Numer. Meth. Fluids, 54: 945963
- [20] Bertagnolio F, Sorensen N, Johansen J ,Profile Catalogue for Airfoil Sections Based on 3D Computations, Riso National Laboratory, 2006